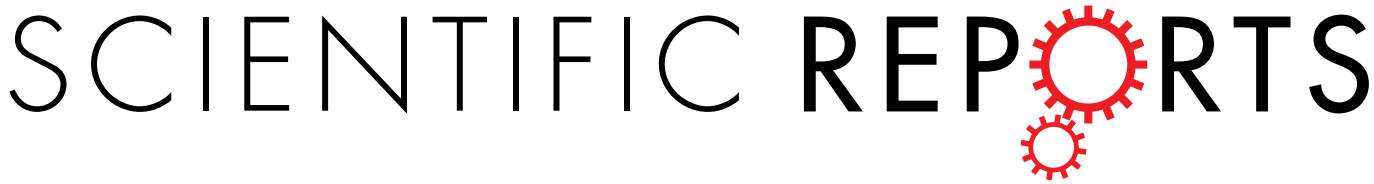

OPEN

Conductive Graphitic Carbon Nitride as an Ideal Material for Electrocatalytically Switchable CO_2 Capture

Received: 13 August 2015
Accepted: 03 November 2015
Published: 01 December 2015

Xin Tan, Liangzhi Kou, Hassan A. Tahini & Sean C. Smith

Good electrical conductivity and high electron mobility of the sorbent materials are prerequisite for electrocatalytically switchable CO_2 capture. However, no conductive and easily synthetic sorbent materials are available until now. Here, we examined the possibility of conductive graphitic carbon nitride (g-C_4N_3) nanosheets as sorbent materials for electrocatalytically switchable CO_2 capture. Using first-principle calculations, we found that the adsorption energy of CO_2 molecules on g-C_4N_3 nanosheets can be dramatically enhanced by injecting extra electrons into the adsorbent. At saturation CO_2 capture coverage, the negatively charged g-C_4N_3 nanosheets achieve CO_2 capture capacities up to 73.9×10^{13} cm^{-2} or 42.3 wt%. In contrast to other CO_2 capture approaches, the process of CO_2 capture/release occurs spontaneously without any energy barriers once extra electrons are introduced or removed, and these processes can be simply controlled and reversed by switching on/off the charging voltage. In addition, these negatively charged g-C_4N_3 nanosheets are highly selective for separating CO_2 from mixtures with CH_4, H_2 and/or N_2. These predictions may prove to be instrumental in searching for a new class of experimentally feasible high-capacity CO_2 capture materials with ideal thermodynamics and reversibility.

At the current rate of emissions of greenhouse gases, for which carbon dioxide (CO_2) is the main component, global warming and climate change will continue to rise[1–3]. One crucial issue facing efficiently separating, capturing, storing and/or converting CO_2 is the development of a practical sorbent material[4–6]. Liquid-amine, which is the most common adsorbent for current industrial process for CO_2 capture, suffers from relatively low efficiency, equipment corrosion, solvent loss, and toxicity[7–10]. Alternatively, various solid materials have been proposed as attractive adsorbents for CO_2 capture, including metal-organic frameworks (MOFs)[11–15], aluminum nitride (AlN)[16], carbon[17–19], hexagonal boron nitride (*h*-BN)[20], and silicon carbide (SiC)[21,22] nanostructures. However, the difficult regeneration processes due to the large adsorption energy, which generally demands high temperatures to release captured CO_2, significantly hinders their practical applications.

Recently, electrocatalytically switchable CO_2 capture scheme has been proposed as a controllable, high selective, and reversible CO_2 capture strategy for bare *h*-BN nanomaterials[23]. Specifically, CO_2 molecules are weakly adsorbed (i.e. physisorbed) on neutral *h*-BN. By injecting extra electrons into *h*-BN adsorbent, density functional theory (DFT) calculations reveal that CO_2 adsorption can be dramatically enhanced via a charge-induced chemisorption interaction. The chemically adsorbed CO_2 can in principle be released when the extra electrons are removed. In contrast to previous methods, the CO_2 capture/release occurs spontaneously once extra electrons are introduced or removed, and the process of CO_2 capture/release can be simply controlled and reversed by switching on/off the charges carried by *h*-BN

Integrated Materials Design Centre (IMDC), School of Chemical Engineering, UNSW Australia, Sydney, NSW 2052, Australia. Correspondence and requests for materials should be addressed to S.C.S. (email: sean.smith@unsw.edu.au)

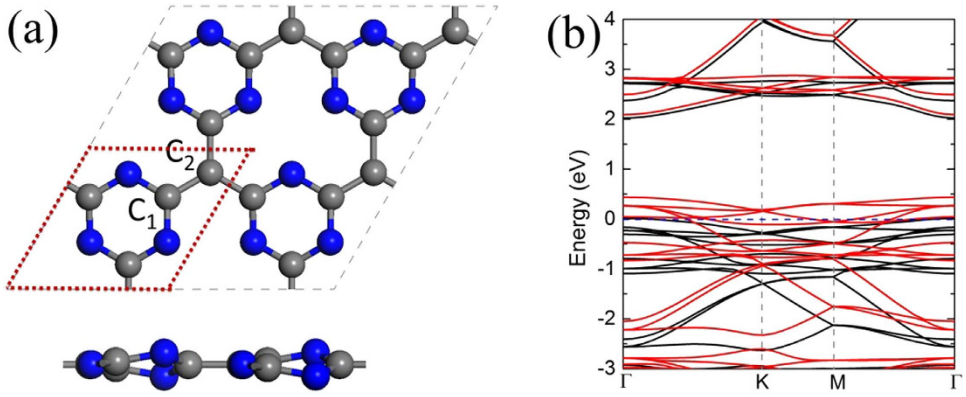

Figure 1. Top (upper) and side (lower) views of (**a**) a (2×2) reconstructed g-C4N3 supercell. The blue and grey balls represent N and C atoms, respectively, and the unit cell of g-C_4N_3 is indicated by red dot lines. C_1 and C_2 denote different C atoms in g-C_4N_3 unit cell. The calculated band structures of (**b**) a (2×2) reconstructed g-C_4N_3. The blue dashed line denotes the Fermi level. The red and black lines in (**b**) denote the spin-up and spin-down states, respectively.

nanomaterials. However, *h*-BN is wide-gap semiconductor with band gap around 5.8 eV[24,25] and it is not clear how to charge up bare *h*-BN due to its insulating character.

To overcome the above disadvantage, Jiao *et al.*[26] have investigated carbon nanotubes with pyridinic-nitrogen as an alternative absorbent to electrocatalytically switchable CO_2 capture because of their good electron conductivity. On the other hand, we have proposed layered *h*-BN and graphene (hybrid BN/G) nanosheets, consisting of a single or double-layer *h*-BN and a substrate graphene layer, as an experimentally feasible approach to induce the requisite charge on *h*-BN for electrocatalytically switchable CO_2 capture[27]. However, the synthesis of carbon nanomaterials with pyridinic nitrogen doping and hybrid BN/G are difficult to control in experiment. One natural question arise: can we find a conductive sorbent material for electrocatalytically switchable CO_2 capture, which avoids complicated synthesis route?

Very recently, intense attention has been attracted by a new class of two-dimensional conjugated polymer, graphitic carbon nitride, due to the anisotropic two-dimensional geometric morphology and the aromatic π-conjugated framework. This endows carbon nitride nanosheets with attractive bandgap- and surface-engineered applications in both energy- and environment-related topics, such as photocatalysis for water splitting[28,29], hydrogen evolution[30], CO2 reduction[31], organosynthesis[32], amongst others[33].g-C_3N_4 and g-C_4N_3 are two kinds of two-dimensional conjugated nanosheets, which have been recently synthesized by using cross-linking nitride-containing anions in ionic liquid[34,35]. Different from each other, g-C_3N_4 is semiconductor[34], while g-C_4N_3 shows half-metallic property[36].

Here we show that electrocatalytically switchable CO_2 capture is indeed possible by considering conductive g-C_4N_3 nanosheets, of which the charge states can be easily modified experimentally because of the good electrical conductivity and high electron mobility. Using first-principle calculations, we found that the adsorption energy of CO_2 molecules on g-C_4N_3 nanosheets can be dramatically enhanced from 0.24 to 2.52 eV by injecting extra electrons into the adsorbent. At saturation CO_2 capture coverage, the negatively charged g-C_4N_3 nanosheets achieve CO_2 capture capacities up to 73.9×10^{13} cm^{-2} or 42.3 wt%. Once the extra electrons are removed, the captured CO_2 molecules can easily desorb from the adsorbent. In contrast to other CO_2 capture approaches, the process of CO_2 capture/release occurs spontaneously without any energy barriers once extra electrons are introduced or removed, and these processes can be simply controlled and reversed by switching on/off the charging voltage. In addition, these negatively charged g-C_4N_3 nanosheets are highly selective for separating CO_2 from mixtures with CH_4, H_2 and/or N_2. These predictions might pave the way in searching for a new class of experimentally feasible high-capacity CO_2 capture materials with ideal thermodynamics and reversibility.

Results

Since good electrical conductivity and high electron mobility are prerequisite for injecting extra electrons into electrocatalytically switchable CO_2 capture materials, we first studied the electronic structures of isolated g-C_4N_3. The lowest-energy configurations and the calculated band structures of g-C_4N_3 are shown in Fig. 1. Consistent with previous studies[36], g-C_4N_3 is a (2×2) reconstructed structure with half-metallic state. This indicates that g-C_4N_3 has good electrical conductivity and high electron mobility, which should readily facilitate electron injection/release for electrocatalytically switchable CO_2 capture.

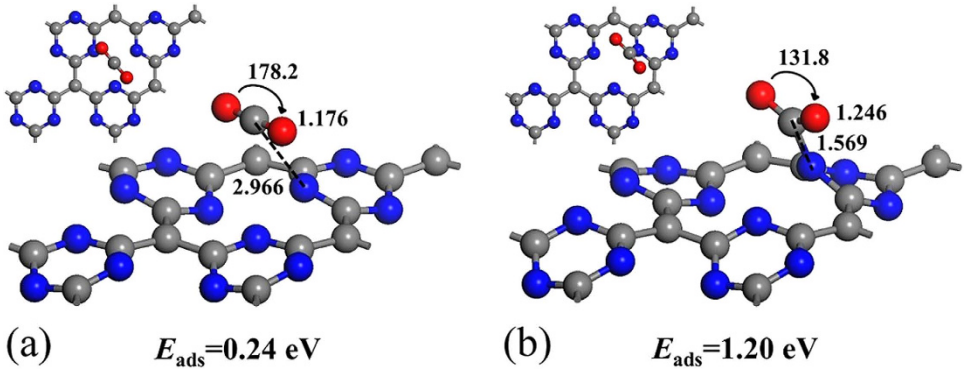

Figure 2. Top and side views of the lowest-energy configurations of a single CO_2 molecule absorbed on the (**a**) neutral and (**b**) 2 e^- negatively charged g-C_4N_3. The blue, grey and red balls represent N, C and O atoms, respectively, and the adsorption energies of the CO_2 molecule on neutral and 2 e^- negatively charged g-C_4N_3 are listed.

Single CO_2 Adsorption on Neutral and 2 e^- Negatively Charged g-C_4N_3 Nanosheets. We next shift our attention to a single CO_2 adsorption on neutral and negatively charged g-C_4N_3. Since g-C_4N_3 is a (2×2) reconstructed structure, there are many different adsorption sites for a CO_2 molecule. Here, we considered all the adsorption sites: directly on top of a C or N atom, above the midpoint of a bond linking the C and N atoms, and above the center of a honeycomb-like hexagon. Figure 2 shows the lowest-energy configurations of a CO_2 absorbed on neutral and 2 e^- negatively charged g-C_4N_3. On neutral g-C_4N_3 (Fig. 2(a)), the linear CO_2 molecule is parallel to g-C_4N_3 and locates on top of three nitrogen atoms. The distance between the C atom of CO_2 and closest N atom is 2.966 Å, and the linear CO_2 molecule shows little structural change compared to a free CO_2 molecule with the O-C-O angle and two double C=O bonds being 178.2° and 1.176 Å, respectively. Mulliken population analysis suggests that the amount of transferred electron from the absorbed CO_2 molecule to g-C_4N_3 is negligible (about 0.004 e^-). For the neutral case, the CO_2 molecule is weakly adsorbed (i.e. physisorbed) onto neutral g-C_4N_3 with small adsorption energy of 0.24 eV.

After injecting two extra electrons into the g-C_4N_3 supercell (Fig. 2(b)), the CO_2 is strongly adsorbed at surface N atom, and changes from physisorption into chemisorption on 2 e^- negatively charged g-C_4N_3. The distance between the C atom of CO_2 and surface N atom of g-C_4N_3 is shortened to 1.569 Å, the O-C-O angle is bent from 178.2° to 131.8°, the two double C=O bonds are elongated from 1.176 to 1.246 Å, and the charge transfer from g-C_4N_3 to CO_2 increase to 0.56e^-. In this case, the adsorption energy of a CO_2 remarkably increases to 1.20 eV, which is much larger than the adsorption energies of CO_2 on other high-performance adsorbents (0.4–0.8 eV)[6], indicating that the negatively charged g-C_4N_3 is an excellent adsorbent for CO_2 capture.

To understand the underlying mechanism of CO_2 capture on negatively charged g-C_4N_3, we plotted the deformation electronic density of neutral and 2 e^- negatively charged g-C_4N_3 by subtracting the electronic density of isolated N and C atoms from the sheet in Fig. 3. Obviously, for the neutral case (Fig. 3(a)), some electrons are extracted from the C atoms and delocalized over the N atoms, as implied by the green regions. Mulliken population analysis indicated that the electrons distribute at N, C_1 and C_2 are −0.302, 0.294 and −0.036 |e|, respectively. When two extra electrons are introduced (Fig. 3(b)), the extra electrons are almost evenly distributed on N and C atoms. Mulliken population analysis suggest that each atom gains $-0.07 \sim -0.09$ |e|, and the electrons distribute at N, C_1 and C_2 are −0.383, 0.222 and −0.122 |e|, respectively. Compared with the neutral case, more electrons are distributed and delocalized at N atoms, as implied by the green regions in Fig. 3(b). As CO_2 is a Lewis acid and it prefers to accept, rather than donate, electrons during reaction, the N atom of negatively charged g-C_4N_3 can donate electrons to CO_2, and form a new bond between the C atom of CO_2 and surface N atom of g-C_4N_3 (Fig. 3(d)), which is significantly different from the case that CO_2 on neutral g-C_4N_3 (Fig. 3(c). This is the reason why the CO_2 molecule has a strong interaction with negatively charged g-C_4N_3.

In order to investigate the kinetic process of CO_2 capture/release on 2 e^- negatively charged g-C_4N_3, we next studied the energy change of a CO_2 molecule adsorbed on g-C_4N_3 after the introduction or removal of the two extra electrons. In Fig. 4(a), we started with the lowest-energy configuration of neutral g-C_4N_3 with a physisorbed CO_2 molecule. Two electrons are then added to the neutral g-C_4N_3, and we examined the energy changes as the system relaxes to the 2 e^- negatively charged optimized state. In Fig. 4(b), we started with the lowest-energy configuration of the 2 e^- negatively charged g-C_4N_3 with a chemisorbed CO_2 molecule. Two electrons are removed, and then the system is allowed to relax, forming a physisorbed CO_2 molecule. When two extra electrons are introduced into g-C_4N_3, the interactions between the CO_2 molecule and the 2 e^- negatively charged g-C_4N_3 are significantly larger than that with neutral g-C_4N_3, and the CO_2 molecule spontaneously relaxes to chemisorption configuration. This

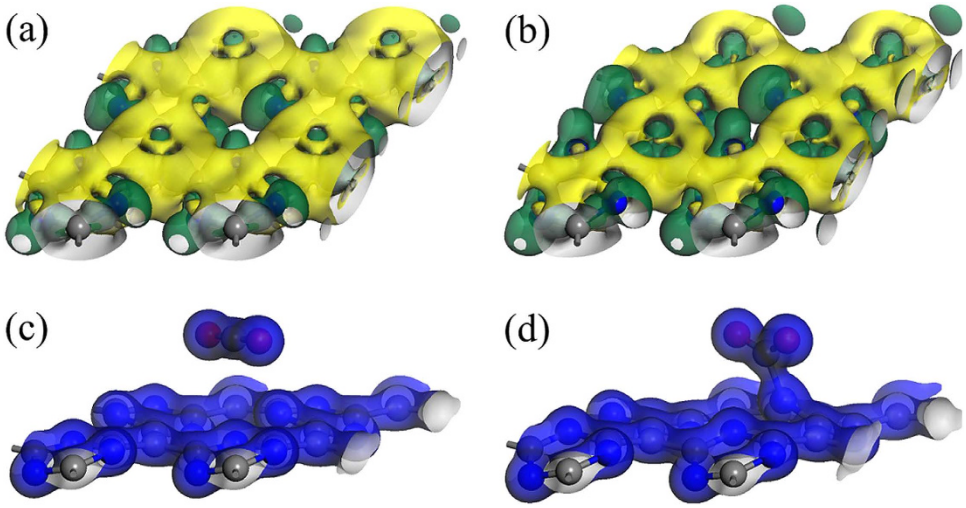

Figure 3. The deformation electronic density of (**a**) neutral and (**b**) 2 e^- negatively charged g-C_4N_3. Green and yellow refer to electron-rich and -deficient area, respectively. The isosurface value is 0.02 e/au. (**c**) The total charge density distribution of a single CO_2 molecule on (**c**) neutral and (**d**) 2 e^- negatively charged g-C_4N_3. The isosurface value is 0.8 e/au. The overlap of the electron densities of the C atom of CO_2 and surface N atom of g-C_4N_3 in (**d**) indicates the formation of a new bond.

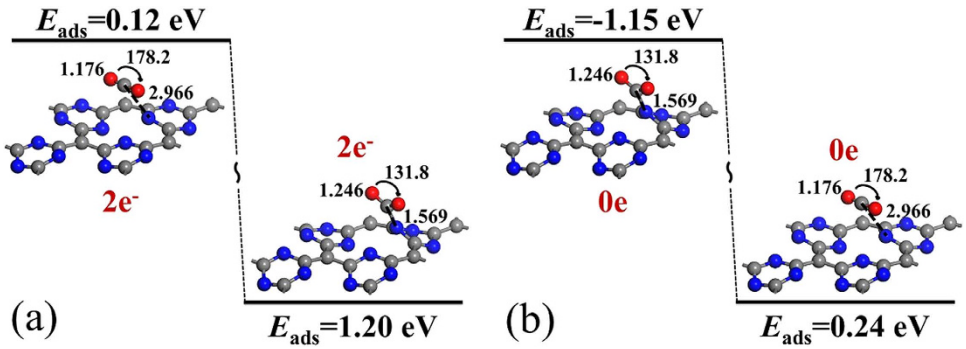

Figure 4. The energy change of (**a**) the relaxation (capture) of a CO_2 molecule on g-C_4N_3 after two extra electrons are introduced, and (**b**) the reverse relaxation (release) process of a captured CO_2 molecule from g-C_4N_3 after two extra electrons are removed from the adsorbent.

process is exothermic by 1.08 eV without any energy barrier. On the other hand, when two extra electrons are removed from the 2 e^- negatively charged g-C_4N_3, the CO_2 molecule spontaneously returns to the weakly bound state and desorbs from g-C_4N_3. This process is also exothermic by 1.39 eV without any energy barrier. Therefore, the CO_2 storage/release processes on negatively charged g-C_4N_3 are reversible with fast kinetics, and can be easily controlled via adding/removing the extra electrons.

The Effects of Charge Density on Single CO_2 Capture on Negatively Charged g-C_4N_3 Nanosheets. To investigate the effects of charge density on CO_2 capture on negatively charged g-C_4N_3, we investigated a CO_2 adsorption on negatively charged g-C_4N_3 with different charge densities. Here, we defined the charge densities of g-C_4N_3 as follows

$$\rho = \frac{Q}{S}$$

where ρ, Q and S are the charge densities of g-C_4N_3, the total charge and the surface area in 2×2 supercell, respectively. For g-C_4N_3, the surface area in 2×2 supercell can be calculated as $S = \frac{\sqrt{3}}{2}a^2$, where a is the lattice constant of 2×2 supercell.

Figure 5 shows the adsorption energies of a CO_2 on negatively charged g-C_4N_3 and the charge transfer between CO_2 and g-C_4N_3 as functions of charge densities. For small charge density case ($< 13.9 \times 10^{13}\,cm^{-2}$), the adsorption energy of CO_2 is small (0.24 ~ 0.35 eV), and charge transfer between

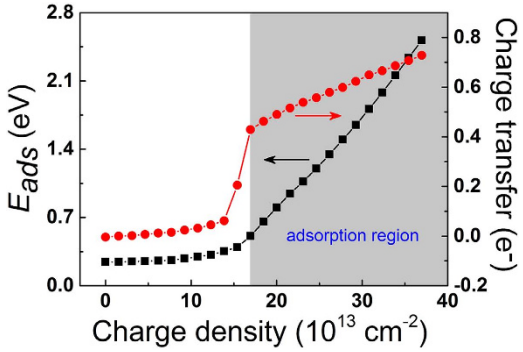

Figure 5. The adsorption energies of a CO_2 on negatively charged g-C_4N_3 and the charge transfer between CO_2 and g-C_4N_3 as functions of charge densities. The gray area indicates the adsorption region.

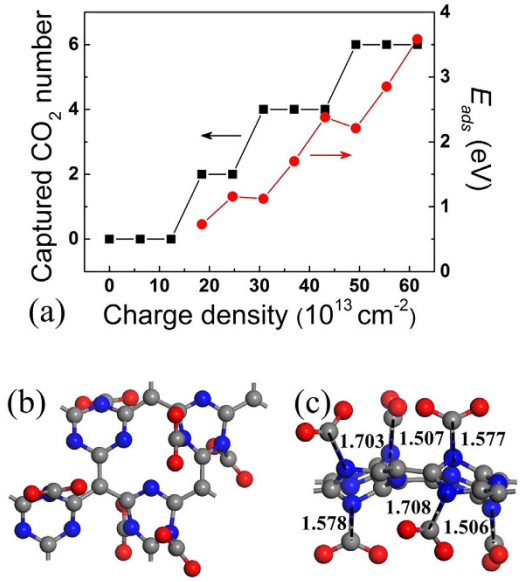

Figure 6. (**a**) The maximum number and the average adsorption energies of captured CO_2 molecules on negatively charged g-C_4N_3 with different charge densities. (**b**) Top and (**c**) side views of the lowest-energy configuration of six CO_2 molecules adsorbed on negatively charged g-C_4N_3 with charge density $61.7 \times 10^{13}\,cm^{-2}$.

CO_2 and g-C_4N_3 is less than 0.06 e^-. When charge density is larger than $13.9 \times 10^{13}\,cm^{-2}$, the adsorption energy of CO_2 and the charge transfer from g-C_4N_3 to CO_2 increase dramatically with increasing charge density, indicating the CO_2 molecule can only adsorb on negatively charged g-C_4N_3 with large charge density. Considering the adsorption energies of CO_2 on other high-performance adsorbents is 0.4−0.8 eV[6], we define the minimum charging density for CO_2 capture on negatively charged g-C_4N_3 is about $17.0 \times 10^{13}\,cm^{-2}$.

CO_2 Capture Capacity on Negatively Charged g-C_4N_3 Nanosheets. To estimate CO_2 capture capacity on negatively charged g-C_4N_3, we studied the maximum number and the average adsorption energy of captured CO_2 molecules on negatively charged g-C_4N_3 with different charge densities (Fig. 6(a)). Here, we determinate the maximum number of captured CO_2 for each negatively charged g-C_4N_3 with different charge density by gradually increasing the number of CO_2 molecules on negatively charged g-C_4N_3 until no more CO_2 can be absorbed. The average adsorption energy of captured CO_2 is calculated as the total adsorption energy divided by the maximum number of captured CO_2. The results show that no CO_2 molecules can be captured by negatively charged g-C_4N_3 with small charge density ($\leq 12.3 \times 10^{13}\,cm^{-2}$). As the charge density increase from 18.5×10^{13} to $61.6 \times 10^{13}\,cm^{-2}$, the negatively charged g-C_4N_3 can capture two, four and six CO_2 molecules with the average adsorption energy of captured CO_2 molecules ranging from 0.72 to 3.58 eV. We note that a further increase in the number of CO_2 molecules leads to some CO_2 molecules moving far away from the adsorbent during the geometry optimization even if we further increase the charge density of g-C_4N_3. Therefore, we define six CO_2

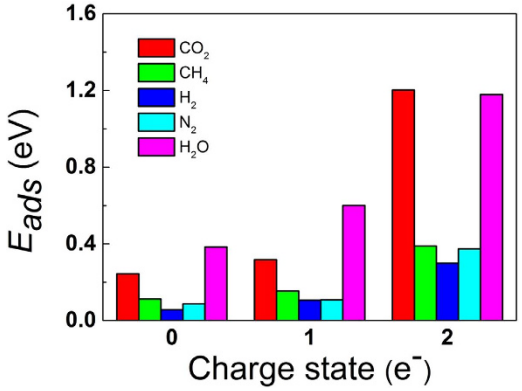

Figure 7. The adsorption energies of CO_2, CH_4, H_2, N_2 and H_2O on neutral, 1 e^- and 2 e^- negatively charged g-C_4N_3.

molecules in each 2 × 2 supercell (i.e. CO_2 capture capacity $73.9 \times 10^{13}\,cm^{-2}$ or 42.3 wt%) as the likely saturation CO_2 capture coverage (Fig. 6(b,c)). It should be noted that surface defective sites such as N vacancies or un-condensed amino group could lower CO_2 capture capacity. However, considering the high CO_2 capture capacity of negatively charged g-C_4N_3, we believe this may nevertheless represent a feasible high-capacity CO_2 capture material.

Interestingly, we note that the CO_2 molecules do not all bind equally but the capture process occurs discretely two at a time. To further confirm this phenomenon, we put four CO_2 molecules on neutral g-C_4N_3 and gradually increase the charge density of negatively charged g-C_4N_3 until four CO_2 are all captured (corresponding lowest-energy configurations are shown in Figure S1 of the Supporting Information). Clearly, four CO_2 are physically adsorbed on neural and 1 e^- negatively charged g-C_4N_3 (Figure S1(a,b), Supporting Information). On 2 e^- negatively charged g-C_4N_3, two CO_2 are chemisorbed while other two CO_2 are physisorbed on adsorbent (Figure S1(c), Supporting Information). When three electrons are introduced, all the CO_2 are captured on 3 e^- negatively charged g-C_4N_3 (Figure S1(d), Supporting Information).

CH_4, H_2 and N_2 Adsorption on g-C_4N_3 Nanosheets. CH_4, H_2, N_2 are three types of gas mixtures that are currently most interesting for CO_2 capture technologies, namely, postcombustion (predominantly CO_2/N_2 separation), natural gas sweetening (CO_2/CH_4), and precombustion (CO_2/H_2) capture[37]. In order to demonstrate the high selectivity of negatively charged g-C_4N_3 nanosheets for CO_2 capture, we calculated the adsorption energies of CH_4, H_2 and N_2 on neutral and negatively charged g-C_4N_3 and compared with those of CO_2. In Fig. 7 we list the comparative adsorption energies of CO_2, CH_4, H_2, and N_2 on neutral, 1 e^- and 2 e^- negatively charged g-C_4N_3 (corresponding lowest-energy configurations are shown in Figure S2 of the Supporting Information). Clearly, the adsorptions of CH_4, H_2 and N_2 on neutral, 1 e^- and 2 e^- g-C_4N_3 are all physical rather than chemical. The distance between the carbon atom of CH_4 (the hydrogen atom of H_2, the nitrogen atom of N_2) and g-C_4N_3 is 3.157–3.159 (2.111–2.539, 2.865–3.236) Å, respectively. The adsorption energies of CH_4, H_2 and N_2 on neutral, 1 e^- and 2 e^- g-C_4N_3 range from 0.06 to 0.39 eV. In contrast, although CO_2 is physically adsorbed at neutral and 1 e^- g-C_4N_3 with small adsorption energy in the range from 0.24 to 0.32 eV, CO_2 is tightly chemisorbed on 2 e^- g-C_4N_3 with large adsorption energy of 1.20 eV. The above comparisons demonstrate that negatively charged g-C_4N_3 has very high selectivity for capturing CO_2 from CH_4, H_2 and/or N_2 mixtures.

Water Adsorption on g-C_4N_3 Nanosheets. Since water saturates most industrial gas streams, including flue gas, we also studied the adsorption energies of H_2O on neutral and negatively charged g-C_4N_3 and compared with those of CO_2, as shown in Fig. 7 (corresponding lowest-energy configurations are shown in Figure S2 of the Supporting Information). On neutral g-C_4N_3, both CO_2 and H_2O are physically adsorbed on adsorbents with small adsorption energies of 0.24 and 0.38 eV, respectively. On 1 e^- g-C_4N_3, the adsorption energy of CO_2 slightly increases to 0.32 eV, while the adsorption energy of H_2O significantly increases to 0.60 eV, which is twice as much as that of CO_2. On 2 e^- g-C_4N_3, both CO_2 and H_2O are chemically adsorbed on adsorbents with large adsorption energies of 1.20 and 1.18 eV, respectively. These results indicate that the negatively charged g-C_4N_3 cannot selectively capture CO_2 from a gas mixture with H_2O present, and we should utilize some absorbent to eliminate water prior to CO_2 adsorption. In fact, since the adsorption energy of H_2O is twice as much as that of CO_2 on 1 e^- g-C_4N_3, utilization of 1 e^- g-C_4N_3 to eliminate water prior to CO_2 adsorption is one potentially viable approach. In this scanario, we could utilize g-C_4N_3 at lower voltage to eliminate water prior to a second stage of CO_2 adsorption at slightly higher voltage.

Discussion

In summary, we have shown that modification of the charge state of conductive g-C_4N_3 nanosheets provides an experimentally feasible approach for electrocatalytically switchable CO_2 capture. Compared with other CO_2 capture approaches, the process of CO_2 capture/release occurs spontaneously without any energy barriers once extra electrons are introduced or removed, and these processes can be simply controlled and reversed by switching on/off the charging voltage. In addition, these negatively charged g-C_4N_3 nanosheets are highly selective for separating CO_2 from mixtures with CH_4, H_2 and/or N_2.

Good electrical conductivity and high electron mobility of the sorbent materials are prerequisite for electrocatalytically switchable CO_2 capture. The aim of the present paper is to explore conductive and easily synthetic sorbent material as an experimentally feasible adsorbent for electrocatalytically switchable CO_2 capture. These predictions may prove to be instrumental in searching for a new class of high-capacity CO_2 capture materials with ideal thermodynamics and reversibility, and we hope that this work will stimulate further theoretical and experimental research in this direction.

Methods

Our DFT calculations employed the linear combination of atomic orbital and spin-unrestricted method implemented in Dmol^3 package[38]. The generalized gradient approximation (GGA) in Perdew-Burke-Ernzerhof (PBE) functional form[39] together with an all-electron double numerical basis set with polarization function (DNP) were adopted. Since the standard PBE functional is incapable of giving an accurate description of weak interactions, we adopted a DFT+D (D stands for dispersion) approach with the Grimme's vdW correction in our computations[40]. The real-space global cutoff radius was set to be 4.1 Å.

To study CO_2 capture/release on g-C_4N_3 nanosheets, we employed 2×2 supercell with periodic boundary conditions in the *x-y* plane (Fig. 1(a)). The vacuum space was set to larger than 20 Å in the *z* direction to avoid interactions between periodic images. In geometry optimizations, all the atomic coordinates were fully relaxed up to the residual atomic forces smaller than 0.001 Ha/Å, and the total energy was converged to 10^{-5} Ha. The Brillouin zone integration was performed on a $(6 \times 6 \times 1)$ Monkhorst-Pack k-point mesh[41].

In order to investigate the gas adsorption on adsorbent, we defined the adsorption energy E_{ads} of CO_2, CH_4, H_2 and N_2 molecules on g-C_4N_3 as follows

$$E_{ads} = (E_{C_4N_3} + nE_{gas} - E_{C_4N_3-gas})/n \quad (1)$$

where $E_{C_4N_3}$, E_{gas}, $E_{C_4N_3-gas}$, and n are the total energy of isolated g-C_4N_3 nanosheets, isolated gas molecule, g-C_4N_3 with the adsorbed gas, and number of gas molecules adsorbed on g-C_4N_3. According to this definition, a more positive adsorption energy indicates a stronger binding of the gas molecule to g-C_4N_3. The electron distribution and transfer mechanism are determined using the Mulliken method[42].

References

1. Jacobson, M. Z. Review of solutions to global warming, air pollution, and energy security. *Energy Environ. Sci.* **2,** 148–173 (2009).
2. Meyer, J. Crisis reading. *Nature* **455,** 733 (2008).
3. Betts, R. A. *et al.* Projected increase in continental runoff due to plant responses to increasing carbon dioxide. *Nature* **488,** 1037–1041 (2007).
4. Haszeldine, R. S. Carbon capture and storage: how green can black be? *Science* **325,** 1647–1652 (2009).
5. Keith, D. W. Why capture CO_2 from the atmosphere? *Science* **325,** 1654–1655 (2009).
6. Chu, S. & Majumdar, A. Opportunities and challenges for a sustainable energy future. *Nature* **488,** 294–303 (2012).
7. Chen, Q. *et al.* Microporous polycarbazole with high specific surface area for gas storage and separation. *J. Am. Chem. Soc.* **134,** 6084–6087 (2012).
8. Zulfiqar, S. *et al.* Amidoximes: promising candidates for CO_2 capture. *Energy Environ. Sci.* **4,** 4528–4531 (2011).
9. Bae, Y.-S. & Snurr, R. Q. Development and evaluation of porous materials for carbon dioxide separation and capture. *Angew. Chem. Int. Ed.* **50,** 11586–11596 (2011).
10. Choi, S., Drese, J. H. & Jones, C. W. Adsorbent materials for carbon dioxide capture from large anthropogenic point sources. *ChemSusChem* **2,** 796–854 (2009).
11. Wang, B., Côte, A. P., Furukawa, H., O'Keeffe, M. & Yaghi, O. M. Colossal cages in zeolitic imidazolate frameworks as selective carbon dioxide reservoirs. *Nature* **453,** 207–211 (2008).
12. Furukawa, H. *et al.* Ultrahigh porosity in metal–organic frameworks. *Science* **329,** 424–428 (2010).
13. Torrisi, A., Bell, R. G. & Mellot–Draznieks, C. Functionalized MOFs for enhanced CO_2 capture. *Cryst. Growth Des.* **10,** 2839–2841 (2010).
14. Liu, J., Thallapally, P. K., McGrail, B. P., Brown, D. R. & Liu, J. Progress in adsorption–based CO_2 capture by metal–organic frameworks. *Chem. Soc. Rev.* **41,** 2308–2322 (2012).
15. Dzubak, A. L. *et al.* Ab initio carbon capture in open–site metal–organic frameworks. *Nat. Chem.* **4,** 810–816 (2012).
16. Jiao, Y., Du, A. J., Zhu, Z. H. & Smith, S. C. A density functional theory study of CO_2 and N_2 adsorption on aluminium nitride single walled nanotubes. *J. Mater. Chem.* **20,** 10426–10430 (2010).
17. Cinke, M., Li, J., Bauschlicher, C. W., Ricca, A. & Meyyappan, M. CO_2 adsorption in single–walled carbon nanotubes. *Chem. Phys. Lett.* **376,** 761–766 (2003).
18. Su, F., Lu, C., Chung, A.-J. & Liao, C.-H. CO_2 capture with amine–loaded carbon nanotubes via a dual–column temperature/vacuum swing adsorption. *Appl. Energy* **113,** 706–712 (2014).
19. Zhang, T., Xue, Q., Zhang, S. & Dong, M. Theoretical approaches to graphene and graphene–based materials. *Nano Today* **7,** 180–200 (2012).

20. Jiao, Y. *et al.* A Density functional theory study on CO_2 capture and activation by graphene–like boron nitride with boron vacancy. *Catal. Today* **175,** 271–275 (2011).
21. Zhao, J.-X. & Ding, Y.-H. Can silicon carbide nanotubes sense carbon dioxide? *J. Chem. Theory Comput.* **5,** 1099–1105 (2009).
22. Zhang, P. *et al.* Curvature effect of SiC nanotubes and sheets for CO_2 capture and reduction. *RSC Adv.* **4,** 48994–48999 (2014).
23. Sun, Q. *et al.* Charge–controlled switchable CO_2 capture on boron nitride nanomaterials. *J. Am. Chem. Soc.* **135,** 8246–8253 (2013).
24. Zunger, A., Katzir, A. & Halperin, A. Optical properties of hexagonal boron nitride. *Phys. Rev. B* **13,** 5560–5573 (1976).
25. Watanabe, K., Taniguchi. T. & Kanda, H. Direct–bandgap properties and evidence for ultraviolet lasing of hexagonal boron nitride single crystal. *Nat. Mater.* **3,** 404–409 (2004).
26. Jiao, Y., Zheng, Y., Smith, S. C., Du, A. & Zhu, Z. Electrocatalytically switchable CO_2 capture: first principle computational exploration of carbon nanotubes with pyridinic nitrogen. *ChemSusChem* **7,** 435–441 (2014).
27. Tan, X., Kou, L. & Smith, S. C. Layered graphene–hexagonal boron nitride nanocomposites: an experimentally feasible approach to charge–induced switchable CO_2 capture. *ChemSusChem* **8,** 2987–2993 (2015).
28. Wang, X. *et al.* A metal-free polymeric photocatalyst for hydrogen production from water under visible light. *Nat. Mater.* **8,** 76–80 (2009).
29. Zhang, J. & Wang, X. Solar water splitting at $\lambda = 600$ nm: a step closer to sustainable hydrogen production. *Angew. Chem. Int. Ed.* **54,** 7230–7232 (2015).
30. Zhang, G. *et al.* Iodine modified carbon nitride semiconductors as visible light photocatalysts for hydrogen evolution. *Adv. Mater.* **26,** 805–809 (2014).
31. Sun, J. *et al.* Bioinspired hollow semiconductor nanospheres as photosynthetic nanoparticles. *Nat. Commun.* **3,** 1139 (2012).
32. Ye, X., Cui, Y. & Wang, X. Ferrocene-modified carbon nitride for direct oxidation of benzene to phenol with visible light. *ChemSusChem* **7,** 738–742 (2014).
33. Zhang, J., Chen, Y. & Wang, X. Two-dimensional covalent carbon nitride nanosheets: synthesis, functionalization, and applications. *Energy Environ. Sci.* doi: 10.1039/C5EE01895A (2015).
34. Kroke, E. *et al.* Tri-*s*-triazine derivatives. Part I. From trichloro-tri-*s*-triazine to graphitic C_3N_4 structures. *New J. Chem.* **26,** 508−512 (2002).
35. Lee, J. S., Wang, X. Q., Luo, H. M. & Dai, S. Fluidic carbon precursors for formation of functional carbon under ambient pressure based on ionic liquids. *Adv. Mater.* **22,** 1004−1007 (2010).
36. Du, A., Sanvito, S. & Smith, S. C. First–principles prediction of metal–free magnetism and intrinsic half–metallicity in graphitic carbon nitride. *Phys. Rev. Lett.* **108,** 197207 (2012).
37. D'Alessandro, D. M., Smit, B. & Long, J. R. Carbon dioxide capture: prospects for new materials. *Angew. Chem. Int. Ed.* **49,** 6058–6082 (2010).
38. Delley, B. From molecules to solids with the $DMol^3$ approach. *J. Chem. Phys.* **113,** 7756–7764 (2000).
39. Perdew, J. P. & Wang, Y. Accurate and simple analytic representations of the electron–gas correlation energy. *Phys. Rev. B* **45,** 13244–13249 (1992).
40. Grimme, S. Semiempirical GGA-Type Density functional constructed with a long-range dispersion correction. *J. Comput. Chem.* **27,** 1787–1799 (2006).
41. Monkhorst, H. J. & Pack, J. D. Special points for brillouin–zone integrations. *Phys. Rev. B* **13,** 5188–5192 (1976).
42. Mulliken, R. S. Electronic population analysis on LCAO–MO molecular wave functions. *J. Chem. Phys.* **23,** 1833–1840 (1955).

Acknowledgements

This research was undertaken with the assistance of resources provided by the National Computing Infrastructure (NCI) facility at the Australian National University; allocated through both the National Computational Merit Allocation Scheme supported by the Australian Government and the Australian Research Council grant LE120100181 ("Enhanced merit-based access and support at the new NCI petascale supercomputing facility, 2012–2015).

Author Contributions

X.T. and S.S. conceived and designed this study, X.T. performed the calculations, L.K. and H.A.T. analyzed data and discussed the results, and all authors contributed to writing the manuscript.

Additional Information

Supplementary information accompanies this paper at http://www.nature.com/srep

Competing financial interests: The authors declare no competing financial interests.

How to cite this article: Tan, X. *et al.* Conductive Graphitic Carbon Nitride as an Ideal Material for Electrocatalytically Switchable CO_2 Capture. *Sci. Rep.* **5**, 17636; doi: 10.1038/srep17636 (2015).